

Unidirectional spin Hall magnetoresistance in ferromagnet/normal metal bilayers

Can Onur Avci, Kevin Garello, Abhijit Ghosh, Mihai Gabureac, Santos F. Alvarado, and Pietro Gambardella

Department of Materials, ETH Zürich, Hönggerbergstrasse 64, CH-8093 Zürich, Switzerland

Magnetoresistive effects are usually invariant upon inversion of the magnetization direction. In noncentrosymmetric conductors, however, nonlinear resistive terms can give rise to a current dependence that is quadratic in the applied voltage and linear in the magnetization. Here we demonstrate that such conditions are realized in simple bilayer metal films where the spin-orbit interaction and spin-dependent scattering couple the current-induced spin accumulation to the electrical conductivity. We show that the longitudinal resistance of Ta|Co and Pt|Co bilayers changes when reversing the polarity of the current or the sign of the magnetization. This magnetoresistance scales linearly with current density and has opposite sign in Ta and Pt, which we associate to the modification of the interface scattering potential induced by the spin Hall effect in these materials. Our results suggest a new route to altering the electric properties of metal films by control of the magnetization.

The effects of the magnetization on the electric conductivity of metals have been studied for a long time¹, providing understanding of fundamental phenomena associated to electron transport and magnetism as well as manyfold applications in sensor technology. The anisotropic magnetoresistance (AMR), the change of the resistance of a material upon rotation of the magnetization, is a prominent manifestation of spin-orbit coupling and spin-dependent conductivity in bulk ferromagnets^{2,3}. In thin film heterostructures, the additional possibility of orienting the magnetization of stacked ferromagnetic layers parallel or antiparallel to each other gives rise to the celebrated giant magnetoresistance (GMR) effect^{4,5}, which has played a major role in all modern developments of spintronics. Together with the early spin injection experiments^{6,7}, the study of GMR revealed how nonequilibrium spin accumulation at the interface between ferromagnetic (FM) and normal metal (NM) conductors governs the propagation of spin currents^{8–11} and, ultimately, the conductivity of multilayer systems^{10,12}.

Recently, it has been shown that significant spin accumulation at a FM/NM interface can be achieved using a current-in-plane (CIP) geometry owing to the spin Hall effect (SHE) in the NM¹³. When FM is a metal and NM is a heavy element such as Pt or Ta, the spin accumulation is strong enough to induce magnetization reversal of nm-thick FM layers at current densities of the order of $j = 10^7 – 10^8$ A/cm² (Refs. 14–16). When FM is an insulator, such as yttrium iron garnet, the SHE causes an unusual magnetoresistance associated to the back-flow of a spin current into the NM when the spin accumulation $\boldsymbol{\mu}_s \sim (\mathbf{j} \times \hat{\mathbf{z}})$ is aligned with the magnetization of the FM, which increases the conductivity of the NM due to the inverse SHE^{17–20}. This so-called spin Hall magnetoresistance (SMR) is characterized by $R^y < R^z \approx R^x$, where R^i is the resistance measured when the magnetization (\mathbf{M}) is saturated parallel to $i = x, y, z$, and differs from the conventional AMR in polycrystalline samples, for which $R = R^x - (R^{y,z} - R^x)[\hat{\mathbf{M}} \cdot \hat{\mathbf{j}}]^2$ and $R^y \approx R^z < R^x$ (Ref. 3).

In this work, we report on a new magnetoresistance effect occurring in FM/NM bilayers with the NM possessing large SHE. The effect combines features that are typical of the current-in-plane (CIP) GMR and SHE, whereby the spin accumulation induced by the SHE in the NM replaces one of the FM polarizers of a typical GMR device. Differently from GMR, however, this effect introduces a nonlinear dependence of the resistance on the current, which gives it unique unidirectional properties: the resistivity changes when reversing either the sign of the magnetization or the polarity of the current, increasing (decreasing) when the

SHE-induced non equilibrium magnetization at the FM/NM interface is oriented parallel (antiparallel) to the magnetization of the FM, as illustrated in Fig. 1a,b. We associate this phenomenon to the modulation of the FM/NM interface resistance due to the SHE-induced spin accumulation, which gives rise to a nonlinear contribution to the longitudinal conductivity that scales proportionally with the current density and has opposite sign in Pt and Ta. Contrary to the linear magnetoresistive effects, including the AMR, GMR, and SMR described above, which are even with respect to the inversion of either the current or magnetization owing to the time reversal symmetry embodied in the Onsager's reciprocity relations, here we observe $R(\mathbf{j}, \mathbf{M}) = -R(-\mathbf{j}, \mathbf{M}) = -R(\mathbf{j}, -\mathbf{M})$, providing a unidirectional contribution to the magnetoresistance in simple bilayer systems.

Sample layout

The samples studied in this work are Pt(1-9nm)|Co(2.5nm) and Ta(1-9nm)|Co(2.5nm) films with spontaneous in-plane magnetization, capped by 2 nm AlO_x and patterned in the shape of Hall bars of nominal length $l = 20 - 50 \mu\text{m}$, width $w = 4 - 10 \mu\text{m}$, and $l/w = 4$, as shown in Fig. 1c. Additional control experiments were carried out on single Co, Ta, and Pt films, and Ta(1,6nm)|Cu(2,4,6nm)|Co(2.5nm) trilayers. To characterize the magnetic and electrical properties of these layers we performed harmonic measurements of the longitudinal resistance (R , see Supplementary Information) and transverse Hall resistance (R_H)^{16,21-23} as a function of a vector magnetic field defined by the polar and azimuthal coordinates θ_B and φ_B . The measurements were carried out at room temperature by injecting an ac current of

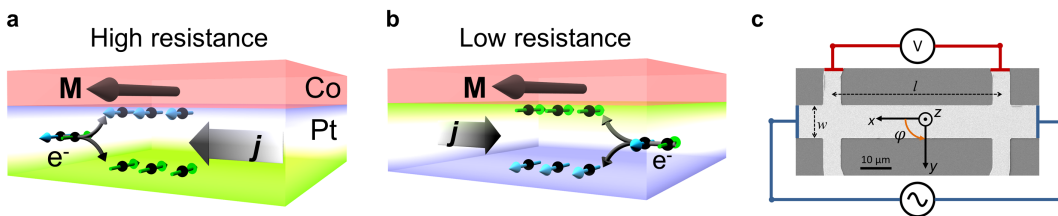


FIG. 1. Illustration of the unidirectional spin Hall magnetoresistance effect and sample layout. **a,** Parallel alignment of the SHE-induced nonequilibrium magnetization at the FM/NM interface with the magnetization of the FM increases the resistivity of the bilayer. **b,** Antiparallel alignment decreases the resistivity. The arrows indicate the direction of the spin magnetic moment. **c,** Scanning electron micrograph of a sample and schematics of the longitudinal resistance measurements.

frequency $\omega/2\pi = 10$ Hz and simultaneously recording the first (R_ω) and second harmonic resistance ($R_{2\omega}$) between the contacts shown in Fig. 1c while rotating the sample in a uniform magnetic field of 1.7 T. Here, R_ω represents the linear response of the samples to the current, that is, the conventional resistance. In order to include the different magnetoresistive angular dependencies in a single expression we write this term as

$$R_\omega = R^z + (R^x - R^z) \sin^2 \theta \cos^2 \varphi + (R^y - R^z) \sin^2 \theta \sin^2 \varphi, \quad (1)$$

where θ and φ are the polar and azimuthal angles of \mathbf{M} , as schematized in Fig. 2a. $R_{2\omega}$ describes resistance contributions that vary quadratically with the applied voltage and includes the current-induced changes of resistivity that are the main focus of this work.

Magnetoresistance measurements

Figure 2b and c show the resistance of Ta(6nm)|Co(2.5nm) and Pt(6nm)|Co(2.5nm) layers during rotation of the applied field in the xy , zx , and zy planes. We observe a sizeable magnetoresistance (MR) in all three orthogonal planes and $R^x > R^z > R^y$ for both samples, in agreement with previous measurements on Pt|Co films^{24,25}. The resistivity of Ta(6nm)|Co(2.5nm) [Pt(6nm)|Co(2.5nm)] is 108.9 (36.8) $\mu\Omega\text{cm}$ and the MR ratios are $(R^x - R^z)/R^z = 0.09\%$ (0.05%) and $(R^z - R^y)/R^z = 0.12\%$ (0.53%). The solid lines represent fits to the MR using Eq. 1 and θ simultaneously measured via the anomalous Hall resistance (see Supplementary Information). In addition to the linear resistance, we measure a significant nonlinear term, $R_{2\omega}$, which has a different angular dependence compared to R_ω and opposite sign in Pt and Ta, as shown in Fig. 2d and e. By fitting the curves with respect to the angles θ and φ (solid lines), we find that $R_{2\omega} \sim \sin\theta \sin\varphi \sim M_y$. In the following, we discuss the type of nonlinear effects that can give rise to such a symmetry.

Spin-orbit torques and thermoelectric contributions

First, we consider oscillations of the magnetization due to the current-induced spin-orbit torques (SOT)^{16,21–23,26}. As the SOT are proportional to the current, ac oscillations of the magnetization can introduce second-order contributions to $R_{2\omega}$ due to the first order MR described by Eq. 1. However, as shown in detail in the Supplementary Information, the SOT-induced signal is not compatible with the angular dependence of $R_{2\omega}$. Both the field-like and antidamping-like SOT (as well as the torque due to the Oersted field) vanish for $\mathbf{M} \parallel y$, where $|R_{2\omega}|$ is maximum. Moreover, the field-like SOT is small in 2.5 nm thick Co

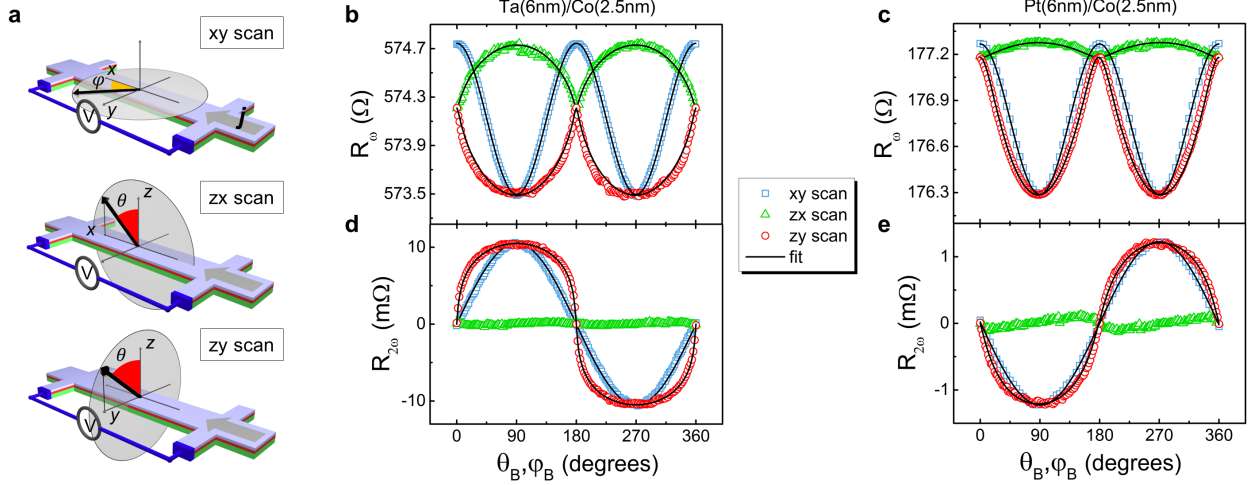


FIG. 2. **Linear and nonlinear magnetoresistance.** **a**, Geometry of the measurements. **b**, First harmonic resistance of Ta(6nm)|Co(2.5nm) and **c**, Pt(6nm)|Co(2.5nm) measured with a current density of $j = 10^7$ A/cm². **d,e** Second harmonic resistance measured simultaneously with **b,c**. The dimensions of the Hall bars are $l = 50$ μ m and $w = 10$ μ m.

layers²³, whereas the antidamping SOT can only induce variations of $R_{2\omega}$ in the zx plane with maxima and minima close to $\theta_B = 0^\circ$ and 180° , which we observe to be small and more pronounced in Pt|Co relative to Ta|Co (Fig. 2b and c bottom panels).

Second, we analyze the influence of thermal gradients (∇T) and related thermoelectric effects. The anomalous Nernst (ANE) and spin Seebeck effect (SSE)^{27,28}, both inducing a longitudinal voltage proportional to $j^2(\mathbf{M} \times \nabla T)$, can give rise to a similar angular dependence as observed for $R_{2\omega}$ when $\nabla T \parallel \hat{\mathbf{z}}$ (see Supplementary Information). Here, we find that thermoelectric voltages are negligible in Pt|Co, in agreement with the very small thermal gradients reported for this system²³. In Ta|Co, on the other hand, the much larger resistivity of Ta relative to Co results in a higher current flowing in the Co layer and a positive ∇T . In such a case, the second harmonic signal of thermal origin, $R_{2\omega}^{\nabla T}$, can be simply estimated from its transverse (Hall) counterpart scaled by the geometric factor l/w when the magnetization is tilted in the x direction, and subtracted from the raw $R_{2\omega}$ signal. Accordingly, we find that $R_{2\omega}^{\nabla T} = 5$ mΩ in Ta(6nm)|Co(2.5nm), which accounts for only about 50% of the total $R_{2\omega}$ reported in Fig. 2. The same procedure applied to Pt|Co gives $R_{2\omega}^{\nabla T}$ mΩ of the order of 5% of the total $R_{2\omega}$, whereas in the control samples lacking a heavy metal we find uniquely a signal of thermal (ANE) origin. We conclude that there is an

additional magnetoresistive effect in the Pt|Co and Ta|Co bilayers that cannot be accounted for by either current-induced magnetization dynamics or thermoelectric voltages.

Unidirectional spin Hall magnetoresistance

The symmetry as well as the opposite sign of this effect in Ta|Co and Pt|Co suggest that it may be related to the scalar product of the magnetization with the SHE-induced spin accumulation at the FM/NM interface, giving rise to a nonlinear MR contribution $R_{2\omega}^{USMR} \sim (\mathbf{j} \times \hat{\mathbf{z}}) \cdot \mathbf{M}$. This relation describes the general features expected from a unidirectional magnetoresistance driven by the spin Hall effect (USMR). We note that this MR contribution depends on the current direction and that the resistance of the bilayer increases when the direction of the majority spins in the FM and the spin accumulation vector are parallel to each other, and decreases when they are antiparallel. This may appear counterintuitive at first sight, considering that the conductivity of Co is larger for the majority spins. However, as we will discuss later, this behavior is consistent with the theory of GMR in FM/NM/FM heterostructures^{10,29,30} when only a single FM/NM interface is retained and the SHE is taken into account.

To investigate further the USMR we have measured $R_{2\omega}$ as a function of an external magnetic field applied parallel to $\hat{\mathbf{y}}$ and current amplitude. Figure 3a shows that $R_{2\omega}$ is constant as a function of field for Ta|Co as well as for Pt|Co (Fig. 3b). In the latter case we observe also two spikes, which we attribute to the magnetization breaking into domains at low field and giving rise to dynamic effects on the domain walls¹⁶. Note that the magnetization of Pt|Co is not fully saturated below 0.65 T due to the large perpendicular magnetic anisotropy of this system, differently from Ta|Co (Supplementary Information). Figure 3c shows the current dependence of $R_{2\omega}^{USMR} = R_{2\omega} - R_{2\omega}^{\nabla T}$ ($R_{2\omega}^{USMR} \approx R_{2\omega}$ for Pt|Co) obtained by taking the average of the data measured at fields larger than $|\pm 1|$ T. $R_{2\omega}^{USMR}$ is linear with the injected current density and converges to zero within the error bar of the linear fit (black lines).

To verify the role of the interfacial spin accumulation due to the SHE we examined the dependence of the USMR on the thickness of the NM. Figure 4a and b show the absolute change of sheet resistance $\Delta R^{USMR} = R_{2\omega}^{USMR}(\pm \mathbf{M}, \pm \mathbf{j}) - R_{2\omega}^{USMR}(\pm \mathbf{M}, \mp \mathbf{j})$ and the relative change of resistivity $\Delta R^{USMR}/R$ measured at constant current density as a function of the Ta and Pt thickness. Both curves exhibit qualitatively similar behavior: an initial sharp

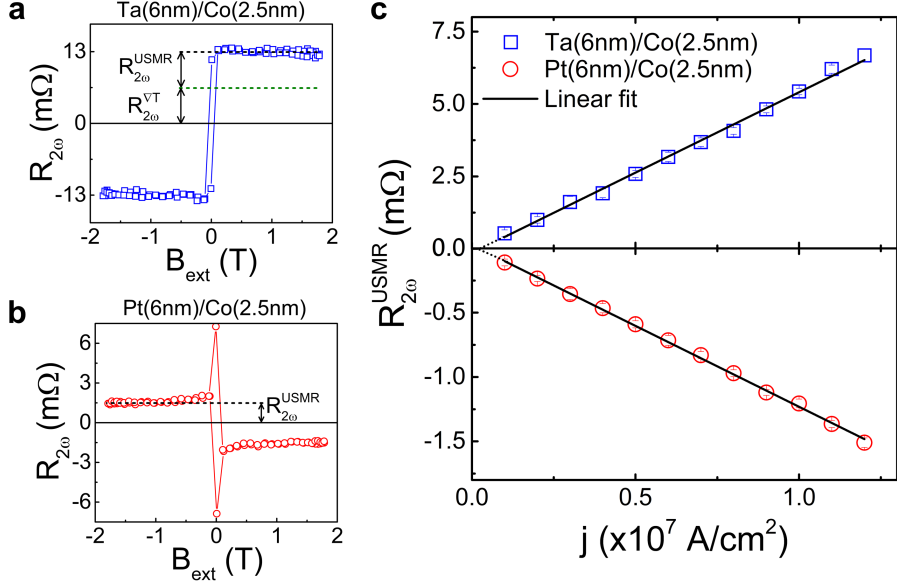


FIG. 3. **Field and current dependence of the nonlinear magnetoresistance.** $R_{2\omega}$ of **a**, Ta(6nm)|Co(2.5nm) and **b**, Pt(6nm)|Co(2.5nm) recorded during a field sweep along y with a current density of $j = 1.2 \cdot 10^7$ A/cm 2 . **c**, Current dependence of $R_{2\omega}^{USMR}$. The solid lines are fits to the data. The slope gives the amplitude of the USMR, which is 5.5 m Ω and 1.25 m Ω per 10 7 A/cm 2 for these samples. The thermal contribution $R_{2\omega}^{\nabla T}$ has been subtracted from the Ta|Co data. The dimensions of the Hall bars are $l = 50$ μ m and $w = 10$ μ m.

increase below 2-3 nm and a gradual decrease as the NM layer becomes thicker. We note that the USMR signal is almost absent in Ta(1nm)|Co, contrary to Pt(1nm)|Co, which we attribute to the oxidation of Ta when deposited on SiO₂ and its consequent poor contribution to electrical conduction. The initial increase of the USMR is consistent with the increment of the spin accumulation at the FM/NM interface as the thickness of the NM becomes larger than the spin diffusion length, which is of the order of 1.5 nm in both Ta and Pt^{31,32}. Moreover, we observe that the decline of the signal in the thicker samples is stronger in Pt|Co than in Ta|Co. This behavior is consistent with Pt gradually dominating the conduction due to its low resistivity, and a smaller proportion of the current experiencing interface scattering in Pt|Co. Conversely, the high resistivity of Ta shunts the current towards the Co side, increasing the relative proportion of the current affected by scattering at the Ta|Co interface.

As an additional check to validate these arguments we have performed measurements on

single Ta(6nm), Pt(6nm), and Co(8nm) layers as well as on Ta(1,6nm)|Cu(2,4,6nm)|Co(2.5nm) trilayers, all capped by 2 nm AlO_x . The USMR is absent in the Ta, Pt, and Co single layers, which also excludes any self induced magnetoresistive effect³³ and proves the essential role of the FM/NM interface. On the other hand, we find a sizable USMR when a Cu spacer is inserted between Ta and Co, which excludes proximity-induced magnetization as a possible cause for the USMR (see Supplementary Information).

Discussion

In order to provide a microscopic explanation for the origin of the USMR we examine the effect of the spin accumulation on the probability of electron scattering at the FM/NM interface. A well-established framework to analyse spin polarized conduction across a FM/NM junction is the two current model, where the minority (spin \uparrow) and majority (spin \downarrow) electron channels are considered separately^{8–10}. As in bulk FM, scattering at the interface is spin-dependent due to the unequal density of majority and minority states near the Fermi level, which, in most cases, leads to a larger resistance for minority electrons relative to majority electrons: $r^\downarrow > r^\uparrow$. This resistance difference is at the heart of the GMR effect, both in the

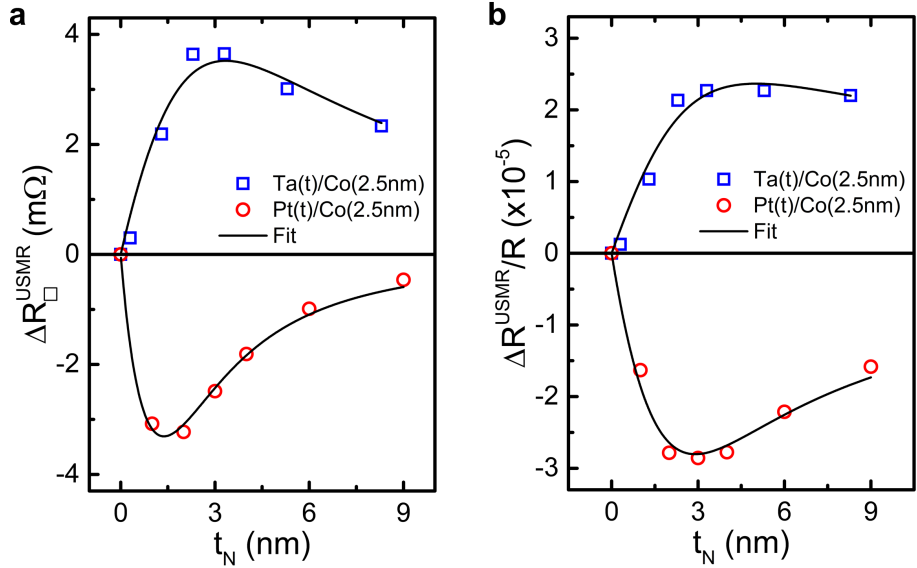


FIG. 4. **USMR as a function of NM thickness.** **a**, Sheet resistance $\Delta R_{2\omega}^{USMR}$ as a function of Ta (squares) and Pt (circles) thickness measured at constant current density $j = 10^7 \text{ A/cm}^2$. The Co layer is 2.5 nm thick in all samples. **b**, Normalized resistance $\Delta R_{2\omega}^{USMR}/R$. The solid lines are fits to the data according to the model described in the text.

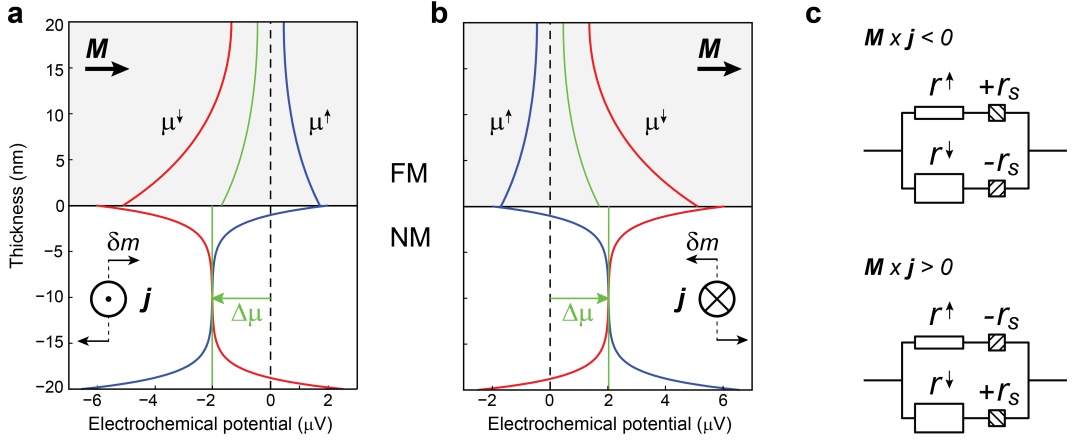


FIG. 5. Modulation of the spin accumulation, spin-dependent electrochemical potential, and interface resistance by the SHE. Profile of the electrochemical potential of majority (μ^\uparrow , blue lines) and minority (μ^\downarrow , red lines) electrons in proximity of the FM/NM interface for **a**, positive and **b**, negative current. The electrochemical potential of the NM shifts relative to that of the FM as indicated by the green arrow. The direction of the magnetization is $\mathbf{M} \parallel \hat{\mathbf{y}}$ in both panels. In our notation, the majority spins are oriented antiparallel to \mathbf{M} and, likewise, the non-equilibrium magnetization induced by the SHE has opposite sign relative to μ_s . Reversing \mathbf{M} is equivalent to exchanging μ^\uparrow and μ^\downarrow and inverting $\Delta\mu$. The sign of the SHE corresponds to Pt|Co; the parameters used to calculate μ^\uparrow and μ^\downarrow are given in the Supplementary Information. **c**, Two current series resistor model of the USMR corresponding to panel **a** (top, higher resistance) and **b** (bottom, lower resistance). Note that the resistances r^\uparrow and r^\downarrow may be generalized to include also the bulk spin-dependent resistances of the FM layer.

CIP^{29,30,34} and the current-perpendicular-to-plane (CPP) geometry^{10,35}. Additionally, when an electric current flows from a FM to a NM or viceversa, another resistance term appears due to the conductivity mismatch between majority and minority electrons on opposite sides of the junction, which results in spin accumulation (Refs. 8 and 9). This so-called "spin-coupled interface resistance", plays a role in CPP-GMR as well as in local and nonlocal spin injection devices^{7,10,36}, whereas in the CIP geometry it is normally neglected because there is no net charge flow across the interface and the spin accumulation is assumed to be zero. If we take the SHE into account, however, the transverse spin current flowing between the NM and the FM induces a splitting of the spin-dependent electrochemical potentials μ^\uparrow and

μ^\downarrow and a net interfacial spin accumulation $\mu_s = \mu^\uparrow - \mu^\downarrow$, which is given by

$$\mu_{s_N} = \mu_{s_N}^0 \tanh \frac{t_N}{2\lambda_N} \frac{1 + \frac{r_b}{\rho_F \lambda_F} (1 - P^2) \tanh \frac{t_F}{\lambda_F}}{1 + \left(\frac{\rho_N \lambda_N}{\rho_F \lambda_F} \coth \frac{t_N}{\lambda_N} - \frac{r_b}{\rho_F \lambda_F} \right) (1 - P^2) \tanh \frac{t_F}{\lambda_F}}, \quad (2)$$

where $\mu_{s_N}^0 = 2e\rho_N\lambda_N\theta_{SH}j$ is the bare spin accumulation due to the SHE that would occur in a single, infinitely thick NM layer, θ_{SH} the spin Hall angle of the NM, $\rho_{N,F}$ and $\lambda_{N,F}$ are the resistivity and spin diffusion length of the NM and FM, respectively, and $r_b = (r^\uparrow + r^\downarrow)/4$ is the interface resistance¹⁰. Moreover, the same effect induces a shift $\Delta\mu = \mu_N - \mu_F$ of the electrochemical potential $\mu_{N,F} = (\mu_{N,F}^+ + \mu_{N,F}^-)/2$ of the NM relative to the FM:

$$\Delta\mu_N = -(P + \gamma\tilde{r})\mu_{s_N}^0 \tanh \frac{t_N}{2\lambda_N} \frac{1}{1 + \frac{\frac{\rho_N \lambda_N}{\rho_F \lambda_F} (1 - P^2) \tanh \frac{t_F}{\lambda_F} \coth \frac{t_N}{\lambda_N}}{1 - \tilde{r}}}, \quad (3)$$

where $\gamma = (r^\downarrow - r^\uparrow)/(r^\uparrow + r^\downarrow)$ and $\tilde{r} = \frac{r_b}{\rho_F \lambda_F} (1 - P^2) \tanh \frac{t_F}{\lambda_F}$. Figure 5a and b show a graphical representation of μ_s and $\Delta\mu_N$; details about the derivation of Eqs. 2 and 3 are given in the Supplementary Information. A key point is that $\Delta\mu_N$ depends on the product $P\theta_{SH}j$, as the USMR, and is linked with the spin-dependent scattering potential that gives rise to different transmission coefficients for majority and minority electrons at the FM/NM interface³⁷. We can thus draw the following qualitative interpretation of the USMR: when the nonequilibrium magnetization induced by the SHE and the magnetization of the FM are parallel to each other ($\delta\mathbf{m} \parallel \mathbf{M}$), the transmission of \uparrow (\downarrow) electrons across the interface is reduced (enhanced) by the accumulation of majority electrons at the FM/NM boundary, due to the conductivity mismatch of \uparrow and \downarrow spins in the two materials. Likewise, when $\delta\mathbf{m} \parallel -\mathbf{M}$, the transmission of \downarrow (\uparrow) electrons across the interface is reduced (enhanced) since minority electrons accumulate at the FM/NM boundary. The overall effect is a modulation of the interface resistance of the \uparrow and \downarrow spin channels by a nonlinear term $\pm r_s$, as schematized in Fig. 5c. This two current (\uparrow and \downarrow) series resistor model shows that such a modulation leads to a resistance difference between the two configurations $\Delta R_{2\omega}^{USMR} \sim 2r_s\gamma$.

Accordingly, using realistic values of r_b , ρ_N , and ρ_F for Ta|Co and Pt|Co, we fit the dependence of the USMR on current and NM thickness to the following phenomenological expression (see Supplementary Information): $\Delta R^{USMR} = A \tanh \frac{t_N}{2\lambda_N} / (1 + R_{FI}/R_N)^2$, where A is a parameter proportional to $P\mu_{s_N}^0$ representing the amplitude of the effect, R_{FI} is the effective resistance of the FM and interface regions, and $R_N = \rho_N l / (w t_N)$ is the resistance of the NM. The denominator accounts for the decreased fraction of electrons that scatter

at the interface as the thickness of the NM increases. Similarly, we obtain $\Delta R^{USMR}/R = (A/R) \tanh \frac{t_N}{2\lambda_N}/(1 + R_{FI}/R_N)$. As shown in Fig. 4, these simple expressions fit ΔR^{USMR} and $\Delta R^{USMR}/R$ remarkably well, providing also values of $\lambda_{Pt} = 1.1$ nm and $\lambda_{Ta} = 1.4$ nm that are in agreement with previous measurements^{31,32}.

This model captures the essential features of the USMR, namely its sign, angular dependence, and proportionality to the current; a more quantitative treatment would require introducing $\Delta\mu$ -dependent reflection and transmission coefficients for electrons impinging on the FM/NM interface in a way analogous to that used to model the CIP-GMR using a semiclassical Boltzmann approach^{29,30}. Here, similarly to the CIP-GMR, the conductivity of the layers is given by an integral over the z - and spin-dependent electronic distribution function with the boundary conditions imposed by interfacial scattering. However, contrary to GMR, there is no need for a second FM layer as the spin polarization is created by the NM via the SHE, which also explains the nonlinear character of the USMR. Detailed calculations including realistic scattering parameters and SHE³⁸ should be able to account for quantitative aspects of the USMR in different materials.

In summary, we found that the SHE adds a nonlinear term to the resistance of FM/NM bilayers that is proportional to $(\mathbf{j} \times \hat{\mathbf{z}}) \cdot \mathbf{M}$ and has the invariance of the cross product $\mathbf{j} \times \mathbf{M}$. Such a term preserves the time-reversal symmetry of the conductivity tensor as both \mathbf{M} and \mathbf{j} are odd under time inversion. The resulting current-voltage ($I - V$) characteristics of the bilayers reads $I = \frac{V}{R}[1 + \frac{R^{USMR}}{R}(\mathbf{j} \times \mathbf{M}) \cdot \hat{\mathbf{z}}]$, where the USMR introduces a quadratic dependence on V . $I - V$ characteristics quadratic in V and linear in the external magnetic field are a general consequence of the simultaneous breaking of time-reversal and inversion symmetry³⁹, and have been observed before in chiral conductors, such as molecular crystals⁴⁰ and metal helices³⁹. However, the nonlinear resistance term in such systems is proportional to $\mathbf{j} \cdot \mathbf{M}$ and has a different symmetry relative to the effect reported here. Finally, we note that nonlinear effects have been evidenced also in CPP-GMR experiments using a dual spin valve geometry⁴¹ and that the USMR is not exclusively linked to the SHE but may arise also due to other sources of nonequilibrium spin accumulation, such as the Rashba effect at FM/NM interfaces and topological insulators^{38,42-44} as well as the anomalous Hall effect in FM. Such effects can be exploited to shed light on the amplitude and origin of the spin accumulation in FM/NM systems and control the electric conductance of spintronic devices in the nonlinear regime.

Methods

This study has been performed on layers with nominal composition of Pt(1-9nm)|Co(2.5nm)|AlO_x(2nm) and Ta(1-9nm)|Co(2.5nm)|AlO_x(2nm) grown by dc magnetron sputtering on thermally oxidized Si wafers. The deposition rates were 0.185 nm/s for Pt, 0.067 nm/s for Ta, 0.052 nm/s for Co, and 0.077 nm/s for Al. The deposition pressure was 2 mTorr and the power was 50 W for all targets. The Al capping layers were oxidized in-situ by a 7 mTorr O₂ plasma at 10 W during 35 s. The continuous layers were then patterned into 6-terminal Hall bars by using standard optical lithography and Ar milling procedures. The Hall bar dimensions are ω for the current line width, $\omega/2$ for the Hall branch width, and $l = 4\omega$ is the distance between two Hall branches, where ω varies between 4 and 10 μm . All layers possess spontaneous isotropic in-plane magnetization with negligible uniaxial magnetic anisotropy. The magnetoresistance and Hall voltage measurements were performed at room temperature by using an ac current modulated at $\omega/2\pi = 10$ Hz, generated by a constant current source. The longitudinal and transverse voltages were recorded simultaneously during 5 s at each angle position in a uniform external field, and fast Fourier transformed to extract the first and second harmonics.

REFERENCES

- ¹W. Thomson, “On the electro-dynamic qualities of metals: Effects of magnetization on the electric conductivity of nickel and of iron,” Proc. R. Soc. London **8**, 546–550 (1856).
- ²I. Campbell, A. Fert, and O. Jaoul, “The spontaneous resistivity anisotropy in Ni-based alloys,” J. Phys. C **3**, S95 (1970).
- ³T. McGuire and R. Potter, “Anisotropic magnetoresistance in ferromagnetic 3d alloys,” IEEE Trans. Magn. **11**, 1018–1038 (1975).
- ⁴M. N. Baibich, J. M. Broto, A. Fert, F. N. Van Dau, F. Petroff, P. Etienne, G. Creuzet, A. Friederich, and J. Chazelas, “Giant magnetoresistance of (001)Fe/(001)Cr magnetic superlattices,” Phys. Rev. Lett. **61**, 2472–2475 (1988).
- ⁵G. Binasch, P. Grünberg, F. Saurenbach, and W. Zinn, “Enhanced magnetoresistance in layered magnetic structures with antiferromagnetic interlayer exchange,” Phys. Rev. B **39**, 4828 (1989).
- ⁶M. Johnson and R. H. Silsbee, “Interfacial charge-spin coupling: Injection and detection

of spin magnetization in metals," Phys. Rev. Lett. **55**, 1790 (1985).

⁷F. Jedema, A. Filip, and B. Van Wees, "Electrical spin injection and accumulation at room temperature in an all-metal mesoscopic spin valve," Nature **410**, 345–348 (2001).

⁸M. Johnson and R. Silsbee, "Thermodynamic analysis of interfacial transport and of the thermomagnetoelectric system," Phys. Rev. B **35**, 4959 (1987).

⁹P. Van Son, H. Van Kempen, and P. Wyder, "Boundary resistance of the ferromagnetic–nonferromagnetic metal interface," Phys. Rev. Lett. **58**, 2271 (1987).

¹⁰T. Valet and A. Fert, "Theory of the perpendicular magnetoresistance in magnetic multilayers," Phys. Rev. B **48**, 7099 (1993).

¹¹S. Maekawa, S. O. Valenzuela, E. Saitoh, and T. Kimura, *Spin Current* (Oxford University Press, 2012).

¹²A. Brataas, G. E. Bauer, and P. J. Kelly, "Non-collinear magnetoelectronics," Phys. Rep. **427**, 157–255 (2006).

¹³J. Sinova, S. O. Valenzuela, J. Wunderlich, C. H. Back, and T. Jungwirth, "Spin Hall effect," <http://arxiv.org/abs/1411.3249>.

¹⁴I. M. Miron, K. Garello, G. Gaudin, P.-J. Zermatten, M. V. Costache, S. Auffret, S. Bandiera, B. Rodmacq, A. Schuhl, and P. Gambardella, "Perpendicular switching of a single ferromagnetic layer induced by in-plane current injection," Nature **476**, 189–193 (2011).

¹⁵L. Liu, C.-F. Pai, Y. Li, H. Tseng, D. Ralph, and R. Buhrman, "Spin-torque switching with the giant spin Hall effect of tantalum," Science **336**, 555–558 (2012).

¹⁶K. Garello, I. M. Miron, C. O. Avci, F. Freimuth, Y. Mokrousov, S. Blügel, S. Auffret, O. Boulle, G. Gaudin, and P. Gambardella, "Symmetry and magnitude of spin-orbit torques in ferromagnetic heterostructures," Nature Nanotech. **8**, 587–593 (2013).

¹⁷H. Nakayama, M. Althammer, Y.-T. Chen, K. Uchida, Y. Kajiwara, D. Kikuchi, T. Ohtani, S. Geprägs, M. Opel, S. Takahashi, *et al.*, "Spin Hall magnetoresistance induced by a nonequilibrium proximity effect," Phys. Rev. Lett. **110**, 206601 (2013).

¹⁸C. Hahn, G. De Loubens, O. Klein, M. Viret, V. V. Naletov, and J. B. Youssef, "Comparative measurements of inverse spin Hall effects and magnetoresistance in YIG/Pt and YIG/Ta," Phys. Rev. B **87**, 174417 (2013).

¹⁹M. Althammer, S. Meyer, H. Nakayama, M. Schreier, S. Altmannshofer, M. Weiler, H. Huebl, S. Geprägs, M. Opel, R. Gross, *et al.*, "Quantitative study of the spin Hall

magnetoresistance in ferromagnetic insulator/normal metal hybrids," Phys. Rev. B **87**, 224401 (2013).

²⁰B. Miao, S. Huang, D. Qu, and C. Chien, "Physical origins of the new magnetoresistance in Pt/YIG," Phys. Rev. Lett. **112**, 236601 (2014).

²¹C. O. Avci, K. Garello, C. Nistor, S. Godey, B. Ballesteros, A. Mugarza, A. Barla, M. Valvidares, E. Pellegrin, A. Ghosh, I. M. Miron, O. Boulle, S. Auffret, G. Gaudin, and P. Gambardella, "Fieldlike and antidamping spin-orbit torques in as-grown and annealed Ta/CoFeB/MgO layers," Phys. Rev. B **89**, 214419 (2014).

²²M. Hayashi, J. Kim, M. Yamanouchi, and H. Ohno, "Quantitative characterization of the spin-orbit torque using harmonic Hall voltage measurements," Phys. Rev. B **89**, 144425 (2014).

²³C. O. Avci, K. Garello, M. Gabureac, A. Ghosh, A. Fuhrer, S. F. Alvarado, and P. Gambardella, "Interplay of spin-orbit torque and thermoelectric effects in ferromagnet/normal-metal bilayers," Phys. Rev. B **90**, 224427 (2014).

²⁴A. Kobs, S. Heße, W. Kreuzpaintner, G. Winkler, D. Lott, P. Weinberger, A. Schreyer, and H. Oepen, "Anisotropic interface magnetoresistance in Pt/Co/Pt sandwiches," Phys. Rev. Lett. **106**, 217207 (2011).

²⁵Y. Lu, J. Cai, S. Huang, D. Qu, B. Miao, and C. Chien, "Hybrid magnetoresistance in the proximity of a ferromagnet," Phys. Rev. B **87**, 220409 (2013).

²⁶J. Kim, J. Sinha, M. Hayashi, M. Yamanouchi, S. Fukami, T. Suzuki, S. Mitani, and H. Ohno, "Layer thickness dependence of the current-induced effective field vector in Ta—CoFeB—MgO," Nature Mater. **12**, 240–245 (2013).

²⁷M. Weiler, M. Althammer, F. D. Czeschka, H. Huebl, M. S. Wagner, M. Opel, I.-M. Imort, G. Reiss, A. Thomas, R. Gross, *et al.*, "Local charge and spin currents in magnetothermal landscapes," Phys. Rev. Lett. **108**, 106602 (2012).

²⁸T. Kikkawa, K. Uchida, Y. Shiomi, Z. Qiu, D. Hou, D. Tian, H. Nakayama, X.-F. Jin, and E. Saitoh, "Longitudinal spin Seebeck effect free from the proximity Nernst effect," Phys. Rev. Lett. **110**, 067207 (2013).

²⁹R. E. Camley and J. Barnas, "Theory of giant magnetoresistance effects in magnetic layered structures with antiferromagnetic coupling," Phys. Rev. Lett. **63**, 664 (1989).

³⁰R. Q. Hood and L. Falicov, "Boltzmann-equation approach to the negative magnetoresistance of ferromagnetic–normal-metal multilayers," Phys. Rev. B **46**, 8287 (1992).

³¹C. Hahn, G. De Loubens, O. Klein, M. Viret, V. V. Naletov, and J. B. Youssef, “Comparative measurements of inverse spin Hall effects and magnetoresistance in YIG/Pt and YIG/Ta,” *Phys. Rev. B* **87**, 174417 (2013).

³²W. Zhang, V. Vlaminck, J. E. Pearson, R. Divan, S. D. Bader, and A. Hoffmann, “Determination of the Pt spin diffusion length by spin-pumping and spin Hall effect,” *Appl. Phys. Lett.* **103**, 242414 (2013).

³³M. Dyakonov, “Magnetoresistance due to edge spin accumulation,” *Phys. Rev. Lett.* **99**, 126601 (2007).

³⁴B. Dieny, “Classical theory of giant magnetoresistance in spin-valve multilayers: influence of thicknesses, number of periods, bulk and interfacial spin-dependent scattering,” *J. Phys. Condens. Matter* **4**, 8009 (1992).

³⁵H. Nguyen, W. Pratt Jr, and J. Bass, “Spin-flipping in Pt and at Co/Pt interfaces,” *J. Magn. Magn. Mat.* **361**, 30–33 (2014).

³⁶S. O. Valenzuela and M. Tinkham, “Direct electronic measurement of the spin Hall effect,” *Nature* **442**, 176–179 (2006).

³⁷S. Zhang, P. Levy, and A. Fert, “Conductivity and magnetoresistance of magnetic multilayered structures,” *Phys. Rev. B* **45**, 8689 (1992).

³⁸P. M. Haney, H.-W. Lee, K.-J. Lee, A. Manchon, and M. Stiles, “Current induced torques and interfacial spin-orbit coupling: Semiclassical modeling,” *Phys. Rev. B* **87**, 174411 (2013).

³⁹G. Rikken, J. Fölling, and P. Wyder, “Electrical magnetochemical anisotropy,” *Phys. Rev. Lett.* **87**, 236602 (2001).

⁴⁰F. Pop, P. Auban-Senzier, E. Canadell, G. L. Rikken, and N. Avarvari, “Electrical magnetochemical anisotropy in a bulk chiral molecular conductor,” *Nature Comm.* **5** (2014).

⁴¹A. Aziz, O. Wessely, M. Ali, D. Edwards, C. Marrows, B. Hickey, and M. Blamire, “Nonlinear giant magnetoresistance in dual spin valves,” *Phys. Rev. Lett.* **103**, 237203 (2009).

⁴²A. Manchon and S. Zhang, “Theory of nonequilibrium intrinsic spin torque in a single nanomagnet,” *Phys. Rev. B* **78**, 212405 (2008).

⁴³I. M. Miron, G. Gaudin, S. Auffret, B. Rodmacq, A. Schuhl, S. Pizzini, J. Vogel, and P. Gambardella, “Current-driven spin torque induced by the Rashba effect in a ferromagnetic metal layer,” *Nature Mater.* **9**, 230–234 (2010).

⁴⁴F. Mahfouzi, N. Nagaosa, and B. K. Nikolić, “Spin-orbit coupling induced spin-transfer torque and current polarization in topological-insulator/ferromagnet vertical heterostructures,” Phys. Rev. Lett. **109**, 166602 (2012).

Acknowledgments

This work was funded by the Swiss National Science Foundation (Grant No. 200021-153404) and the European Commission under the 7th Framework Program (SPOT project, Grant No. 318144).

Author contributions

C.O.A., K.G., and P.G. planned the experiments; M.G., A.G., S.F.A., and C.O.A. carried out the sample growth and patterning; C.O.A., K.G., and A.G. performed the measurements; C.O.A. and P.G. analyzed the data and wrote the manuscript. All authors contributed to the discussion of the data in the manuscript and Supplementary Information.

Additional information

Correspondence and requests for materials should be addressed to
C.O.A. (can.onur.avci@mat.ethz.ch) and P.G. (pietro.gambardella@mat.ethz.ch).